

# Traffic of interacting ribosomes on mRNA during protein synthesis: effects of chemo-mechanics of individual ribosomes

Aakash Basu<sup>1</sup> and Debashish Chowdhury\*<sup>1</sup>

<sup>1</sup>*Department of Physics, Indian Institute of Technology, Kanpur 208016, India.*

(Dated: September 5, 2018)

Many *ribosomes* simultaneously move on the same messenger RNA (mRNA), each synthesizing a protein. In contrast to the earlier models, here *we develop a “unified” theoretical model* that not only incorporates the *mutual exclusions* of the interacting ribosomes, but also describes explicitly the mechano-chemistry of each of these individual cyclic machines during protein synthesis. Using a combination of analytical and numerical techniques of non-equilibrium statistical mechanics, we analyze the rates of protein synthesis and the spatio-temporal organization of the ribosomes in this model. We also predict how these properties would change with the changes in the rates of the various chemo-mechanical processes in each ribosome. Finally, we illustrate the power of this model by making experimentally testable predictions on the rates of protein synthesis and the density profiles of the ribosomes on some mRNAs in *E-coli*.

PACS numbers:

## I. INTRODUCTION

Genetic information is stored in the sequence of nucleotides on each single strand of deoxyribonucleic acid (DNA). Proteins are polymers of amino acids. The synthesis of proteins from DNA takes place in several stages [1]. The two main stages in this sequence are: (i) *transcription*, where the messenger RNA (mRNA) is synthesized using the template provided by a single-stranded DNA; and (ii) *translation* where the codons (triplets of nucleotides) on the mRNA are sequentially decoded and a protein (or, more precisely, a polypeptide) is synthesized. These two stages may, however, overlap and translation of a mRNA can begin even before transcription is completed [2]. Translation is carried out by the ribosome [3]. From the perspective of physics, ribosome is one of the largest and most sophisticated *macromolecular machines* within the cell [4]; it is essentially a “protein-making motor protein” [5] that consumes chemical energy for its mechanical movements [6]. In this paper we focus exclusively on *translation* by ribosomes.

Most often many ribosomes move simultaneously on the same mRNA strand while each synthesises a protein. It has been realized for a long time that the inter-ribosome interactions cannot be ignored except at extremely low densities. The collective movement of ribosomes on a single mRNA strand has superficial similarities with vehicular traffic [7, 8, 9, 10] and, therefore, will be referred to as ribosome traffic. Our main aim is to develop a theoretical model of the collective movement of the ribosomes on a mRNA strand as well as to investigate the interplay of intra-ribosomal chemo-mechanics and inter-ribosome interactions.

In all the earlier models of ribosome traffic [11, 12, 13, 14, 15, 16, 17, 18, 19], the entire ribosome is modelled

as a single “self-propelled particle” ignoring its molecular composition and architecture. Moreover, in these models the inter-ribosome interactions are captured through hard-core mutual exclusion. Furthermore, the dynamics of the system is formulated in terms of rules that are essentially straightforward extensions of the totally asymmetric simple exclusion process (TASEP) [20]. In the TASEP a particle can hop forward to the next lattice site, with a probability  $q$  per time step, if and only if the target site is empty; updating is done throughout either in parallel or in the random-sequential manner. In fact, TASEP is one of the simplest models of systems of interacting driven particles [21, 22]. The TASEP-like earlier models of ribosome traffic capture the effects of all the chemical reactions and conformational changes, which lead to the translocation of a ribosome from one codon to the next, by a single parameter, namely, the probability of hopping, per unit time, of a ribosome from one lattice site to the next.

In reality, as mentioned earlier, a ribosome is a molecular motor whose mechanical movement is coupled to its biochemical cycle. In this paper we develop a model that not only incorporates the inter-ribosome steric interactions (mutual exclusion), but also captures explicitly the essential steps in the intra-ribosome chemo-mechanical processes, including peptide bond formation and translocations driven by GTP (guanine triphosphate) hydrolysis.

Our modelling strategy for incorporating the biochemical cycle of ribosomes is similar to that followed in the recent work [23] on single-headed kinesin motors KIF1A. However, the implementation of the strategy is more difficult here not only because of the higher complexity of composition, architecture and mechano-chemical processes of the ribosomal machinery and but also because of the sequence *heterogeneity* of the mRNA track [24, 25]. Our modelling strategy has enabled us to achieve a synthesis- in the low-density limit, our model accounts for the protein synthesis by a single isolated ribosome

---

\*Corresponding author(E-mail: debch@iitk.ac.in)

while at higher densities the same model predicts not only the rate of protein synthesis but also the collective density profile of the ribosomes on the mRNA strand.

Our approach is based on a stochastic chemical kinetic model which makes no commitments to either power stroke or Brownian ratchet mechanism [26, 27, 28] of molecular motors. The main quantities of our interest are the rates of protein synthesis and the density profile of the ribosomes on the mRNA strand. Both these have played key roles in the studies of dynamical phases and boundary-induced non-equilibrium phase transitions in driven-diffusive lattice gas models [20, 22]. But, in contrast to the earlier models of ribosome traffic, we explore the dependence of these quantities on the rate constants for various steps of its chemo-mechanical cycle in real time and also plot the phase diagrams in planes spanned by experimentally accessible parameters.

The paper is organized as follows: Because of the interdisciplinary nature of the topic investigated in this paper, we present in section II a summary of the essential biochemical and mechanical processes during a complete operational cycle of a single ribosome. We present a brief critical review of the earlier models in section III followed by a description of our model in section IV so as to highlight the novel features of our model. We report our results on this model with periodic boundary conditions in sections V and VI and those with open boundary conditions in section VII. We summarize the main results and draw conclusions in section VIII.

## II. SUMMARY OF THE ESSENTIAL CHEMO-MECHANICAL PROCESSES

The process of translation itself can be divided into three main stages: (a) *initiation*, during which the ribosomal subunits assemble on the initiator codon on the mRNA strand, (b) *elongation*, during which the nascent polypeptide gets elongated by the formation of peptide bonds with new amino acids, and (c) *termination*, during which the process of translation gets terminated at the stop codon and the polypeptide is released. In this paper we shall be concerned mostly with the process of *elongation*.

Each ribosome consists of two parts which are usually referred to as the larger and the smaller subunits. There are four binding sites on each ribosome. Of these, three sites (called E, P, A), which are located in the larger subunit, bind to aa-tRNA, while the fourth binding site, which is located on the smaller subunit, binds to the mRNA strand. The translocation of the smaller subunit of each ribosome on the mRNA track is coupled to the biochemical processes occurring in the larger subunit. The chemo-mechanical cycle of a ribosome is drawn in fig.1 and three major steps in this cycle are sketched schematically in fig.2.

Let us begin the biochemical cycle in the elongation phase with state 1, (figure 1) where a tRNA is bound

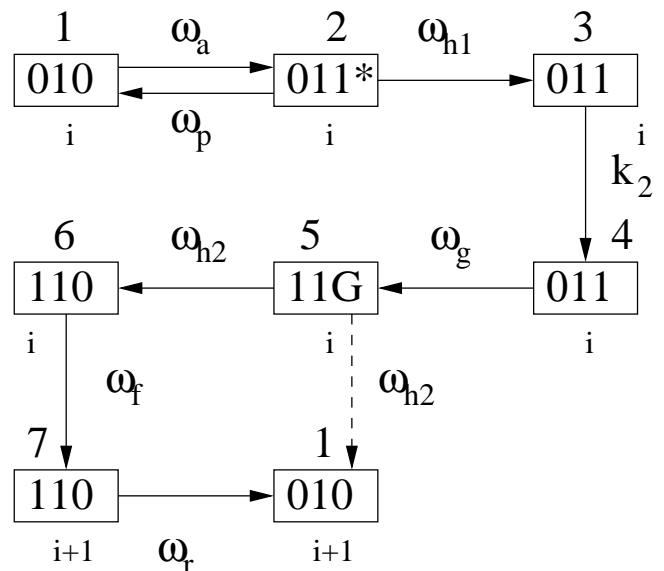


FIG. 1: A schematic representation of the biochemical cycle of a single ribosome during the elongation stage of translation in our model. Each box represents a distinct state of the ribosome. The index below the box labels the codon on the mRNA with which the smaller subunit of the ribosome binds. The number above the box labels the biochemical state of the ribosome. Within each box, 1(0) represents presence (absence) of tRNA on binding sites E, P, A respectively. 1\* is a EF-Tu bound tRNA and G is a EF-G GTPase. The symbols accompanied by the arrows define the rate constants for the transitions from one biochemical state to another. As explained in section IV, the dashed arrow represents the approximate pathway we have considered in the simplified dynamics of our model.

to the site P. A tRNA-EF-Tu complex now binds to site A and the system makes a transition from the state 1 to the state 2. As long as the EF-Tu is attached to the tRNA, codon-anticodon binding can take place, but the peptide bond formation is prevented. The EF-Tu has a GTP part which is hydrolyzed to GDP, driving the transition from state 2 to 3. Following this, a phosphate group leaves, resulting in the intermediate state 4. This hydrolysis, finally, releases the EF-Tu, and the peptide bond formation is now possible. After this step, EF-G, in the GTP bound form, comes in contact with the ribosome. This causes the tRNAs to shift from site P to E and from site A to P, site A being occupied by the EF-G, resulting in the state 5. Hydrolysis of the GTP to GDP then releases the EF-G and this is accompanied by the transition of the system from the state 5 to the state 6. The transition from the state 6 to state 7 is accompanied by conformatinal changes that are responsible for pulling the mRNA-binding smaller subunit by one step forward. Finally, the tRNA on site A is released, resulting in the completion of one biochemical cycle; in the process the ribosome moves forward by one codon (i.e., one step on the lattice).

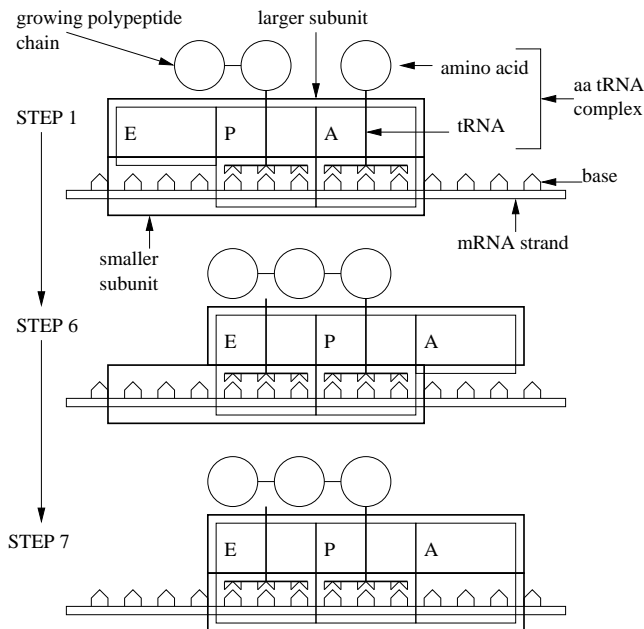


FIG. 2: A pictorial depiction of three major steps in the chemo-mechanical cycle of a single ribosome. The larger and smaller subunits have been depicted as two rectangles. The complementary shapes of the vertical tips and dips merely emphasize the codon-anticodon matching.

### III. BRIEF REVIEW OF THE EARLIER MODELS

To our knowledge, MacDonald, Gibbs and coworkers [11, 12] developed the first quantitative theory of simultaneous protein synthesis by many ribosomes on the same mRNA strand. Their model is shown schematically in fig.3. The sequence of the codons on a given mRNA was represented by the corresponding sequence of the equispaced sites of a regular one-dimensional lattice. Each of the ribosomes was modelled by a self-propelled particle of size  $\ell$  in the units of the lattice constant; thus,  $\ell$  is an integer. On the lattice the steric repulsion of the ribosomes was taken into account by imposing the condition of mutual exclusion, i.e., no site of the lattice can be simultaneously covered by more than one particle.

The dynamics of the system was formulated in terms of the following update rules:

An extended particle (effectively, a *hard rod*), whose forward edge is located at the site  $i$ , can hop forward by one lattice spacing with the forward hopping rate  $q^{(i)}$  provided the target site is not already covered another extended particle. Moreover, initiation and termination were assumed to take place with the corresponding rates  $\alpha$  and  $\beta$ , respectively, which are not necessarily equal to any of the other rate constants. For the sake of simplicity of analytical calculations, it was assumed [11, 12] that  $q^i = q$ , irrespective of  $i$ . This, effectively, replaces an intrinsically inhomogeneous process by a homogeneous one

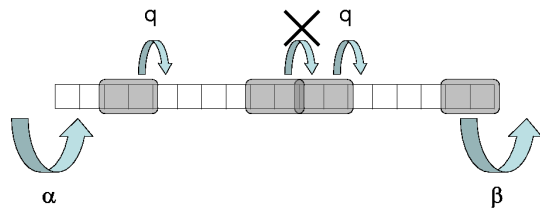


FIG. 3: Schematic representation of TASEP-type models of protein synthesis. The lattice of rectangular cells represents the codon sequence on a mRNA while each rectangular block of length  $\ell$  (in this figure  $\ell = 2$ ) denotes an “extended particle” which represents a ribosome.

which ignores the dependence of the biochemical steps on the codon or on the corresponding tRNA. In such special situations, this model reduced to TASEP without any defect or disorder, except that the allowed size of the “extended” hopping particles are multiples of the lattice spacing.

Periodic boundary conditions are less realistic than open boundary conditions for capturing protein synthesis by a theoretical model. Nevertheless, if one imposes periodic boundary conditions on this simplified version of the model, the steady-state solution is uniform, i.e., the probability of finding the ribosome at a given site is independent of the site  $i$ . The steady-state flux  $J$  of the ribosomes is defined as the average number of the ribosomes crossing an arbitrary codon per unit time. In the steady-state corresponding to periodic boundary conditions, the flux of the ribosomes, in the absence of any backward hopping, is given by [11, 29]

$$J = q \left[ \frac{\rho(1 - \rho \ell)}{1 - \rho(\ell - 1)} \right] \quad (1)$$

where  $\rho$  is the number density of the ribosomes; if  $N$  is the total number of ribosomes on the lattice of length  $L$ , then  $\rho = N/L$ . The corresponding average speed of the ribosomes is given by  $\langle v \rangle = J/\rho$ . Comparing equation (1) with the corresponding expression

$$J = q \rho(1 - \rho) \quad (2)$$

for the steady-state flux in the TASEP,  $\rho/[1 - \rho(\ell - 1)]$  has often been identified [30] as an *effective* particle density while the corresponding *effective* hole density is given by  $1 - \rho\ell$ . The corresponding phenomenological hydrodynamic theory [14] has also been derived [31, 32] from the

TASEP-like dynamics of the hard rods of size  $\ell$  on the discrete lattice.

Because of the close analogy with vehicular traffic, we shall refer to the flux-density relation as the fundamental diagram [7]. The fundamental diagram implied by the expression (1) exhibits a *maximum* at the density  $\rho_m$  and the value of flux at this maximum is  $J_m$  where

$$\rho_m = \frac{1}{\sqrt{\ell}(\sqrt{\ell} + 1)} \quad \text{and} \quad J_m = \frac{q}{(\sqrt{\ell} + 1)^2}. \quad (3)$$

Only in the special case  $\ell = 1$ , this fundamental diagram is symmetric about  $\rho = 1/2$  which is referred to as the particle-hole symmetry in the traffic literature [7]; the maximum shifts to higher density with increasing  $\ell$ .

The ribosome density profile in the model developed by Macdonald et al. has been investigated in detail by solving the equations numerically [11, 12, 33]. Similar results on the synthesis rate, ribosome density profile and several other interesting quantities have been calculated either by numerical solution of the equations or by carrying out direct computer simulations of this model as well as some other closely related models [34, 35, 36, 37, 38, 39].

None of the existing quantitative models mentioned above distinguishes between the larger and the smaller subunits of the ribosome. Instead, in those models, the entire macromolecular machine is represented by a single “extended particle”. Moreover, the simple dynamics does not account for the detailed biochemical cycle of each single ribosome and how these chemical reactions drive its translocation from one codon to the next one. Instead, the entire complexity of its mechano-chemistry is captured by one single parameter, namely, the effective probability  $q$  of its hopping forward from one lattice site to the next, which is equivalent to the rate constant for the forward reaction that elongates the protein by one amino acid.

## IV. THE MODEL

### A. Components, structures and architectures

The model is shown schematically in fig.4. Our model differs from all earlier models in the way we capture the structure, biochemical cycle and translocation of each ribosome. But, our strategy for modelling the mRNA is exactly identical to that followed in the literature since the pioneering work of MacDonald, Gibbs and coworkers [11, 12].

We represent the single-stranded mRNA chain, consisting of  $L$  codons, by a one-dimensional lattice of length  $L + \ell - 1$  where each of the first  $L$  sites from the left represents a single codon. We label the sites of the lattice by the integer index  $i$ . The left-to-right sequence of the sites represent the codon sequence from 5'-to-3' end of the mRNA and, therefore, each ribosome moves from left to right on the lattice; the site  $i = 1$  represents the

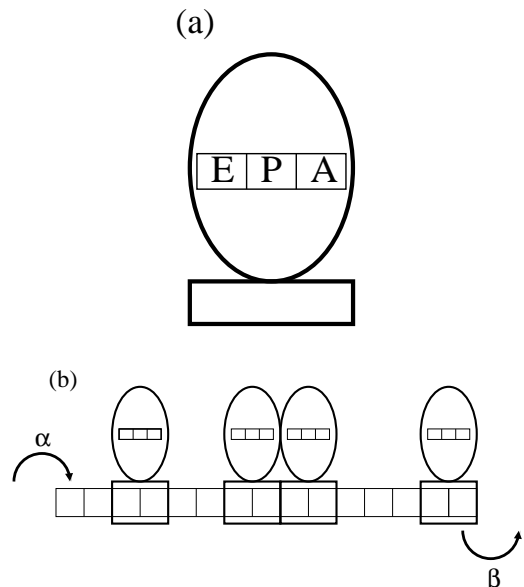


FIG. 4: A schematic representation of the model. (a) A cartoon of a single ribosome that explicitly shows the three binding sites E, P and A on the larger subunit which is represented by the ellipsoidal lobe. The rectangular lower part represents the smaller subunit of the ribosome. (b) The mRNA is represented as a one-dimensional lattice where each site corresponds to one single codon. The smaller subunit of each ribosome covers  $\ell$  codons ( $\ell = 2$  in this figure) at a time.

start codon while the site  $i = L$  corresponds to the stop codon.

To begin with, we shall consider a perfectly periodic lattice with identical sites. This simplified situation is similar to the homogeneous template considered in the pioneering works in ref.[11, 12] and most of the subsequent works in the literature. However, in this paper, we shall also model protein synthesis in *E-coli* using the actual sequence of codons in a few mRNAs transcribed from real genes which are intrinsically inhomogeneous.

In principle, during actual translation it may be necessary first to unwind the mRNA, at least locally, to get access to the codon sequence on a single-stranded mRNA. Interestingly, the ribosome itself exhibits helicase activity for this purpose [40]; this function is somewhat similar to the helicase activity of the RNA polymerase which is known to unwind double-stranded DNA during transcription. However, we shall not include this helicase activity of the ribosome explicitly in our model and assume that an active ribosome translocates on an effectively one-dimensional lattice.

The small sub-unit of the ribosome, which is known to bind with the mRNA, is represented by an *extended particle* of length  $\ell$  which is expressed in the units of the size of a codon (see fig.4). We assume the simplest form of mutual interactions among the ribosomes. These do not interact if they do not touch each other. However, if two ribosomes touch each other, the leading ribosome

(which contains a longer nascent protein) will be assumed to be totally unaffected by the following ribosome while the following ribosome will fail to move forward as long as the leading one remains in its current position. Thus, in our model, the small subunit of each ribosome covers  $\ell$  codons at a time; no lattice site is allowed to be covered simultaneously by more than one overlapping ribosome. Irrespective of the length  $\ell$ , each ribosome moves forward by only one site in each step as it must translate successive codons one by one.

### B. Dynamics of the model

The initiation step is known to be the rate-limiting process for translation of many mRNAs and involves many regulatory molecules. But, since our model is *not* intended to describe initiation in detail, we represent initiation by a single parameter  $\alpha$ . Whenever the first  $\ell$  sites on the mRNA are vacant this group of sites is allowed to be covered by a ribosome, from the pool of unbound ribosomes, with the probability  $\alpha$  in the time interval  $\Delta t$  (in all our numerical calculations we take  $\Delta t = 0.001$  s). Since  $\alpha$  is the probability of attachment in time  $\Delta t$ , the probability of attachment per unit time (which we call  $\omega_\alpha$ ) is the solution of the equation  $\alpha = 1 - e^{-\omega_\alpha \times \Delta t}$  (see appendix A for the detailed explanation).

Similarly, since we are not interested in modelling the termination of translation with all the molecular level processes in detail, we describe termination in our model by a single parameter  $\beta$ ; whenever the rightmost  $\ell$  sites of the mRNA lattice are covered by a ribosome, i.e., the ribosome is bound to the  $L$ -th codon, the ribosome gets detached from the mRNA with probability  $\beta$  in the time interval  $\Delta t$ .

So far as the elongation stage is concerned, all the earlier models describe elongation of the protein by one amino acid also in terms of a single parameter, namely, the rate  $q$  of hopping of a ribosome from one codon to the next. In contrast, we model the chemo-mechanics of elongation in detail.

In the elongation stage, we have identified *seven* distinct states of the ribosome in each cycle which have been described in detail in section II (shown schematically in fig.1). It is possible that there are transient intermediate states and each step mentioned above may have to be divided into substeps. Although, in principle, our model can be trivially extended to incorporate such finer details, we do not attempt such extensions of the model here. Instead, in setting up the equations below, we simplify the model. Throughout this paper, we do not consider explicitly the transitions  $5 \rightarrow 6$ ,  $6 \rightarrow 7$  and  $7 \rightarrow 1$ . We replace the pathway  $5 \rightarrow 6 \rightarrow 7 \rightarrow 1$  by an effectively direct single transition  $5 \rightarrow 1$ , with rate constant  $\omega_{h2}$  (shown by the dashed line in fig.1). This simplification is justified by the fact that the transitions  $5 \rightarrow 6$  and  $6 \rightarrow 7$  are purely “chemical”, and do not seem to depend on the availability of elongation factors, or GTP or aa-

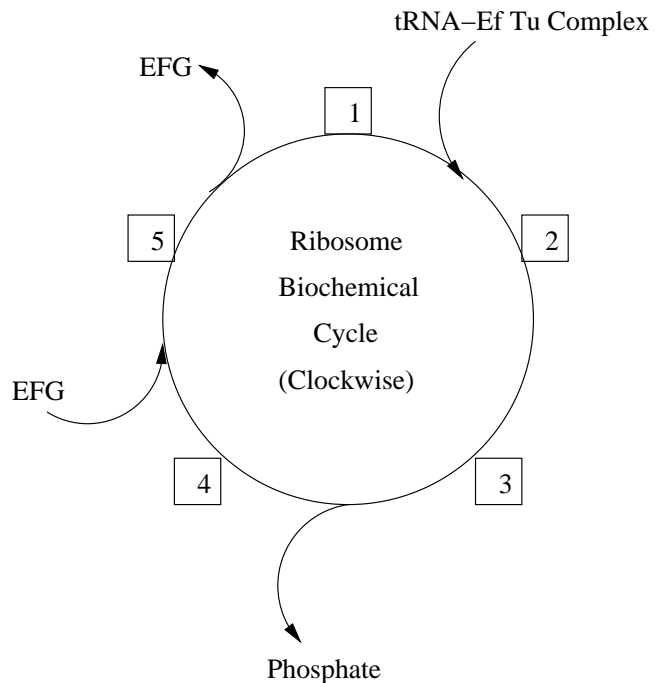


FIG. 5: Simplified version of the full biochemical cycle shown in figure 1. Each box represents a state, and the numbering is the same as in figure 1. See text in section IV for justification in favour of using this simplified dynamics in our model.

$\omega_\alpha$ ( $s^{-1}$ )	$\omega_g$ ( $s^{-1}$ )	$\omega_p$ ( $s^{-1}$ )	$\omega_{h1}$ ( $s^{-1}$ )	$\omega_{h2}$ ( $s^{-1}$ )	$k_2$ ( $s^{-1}$ )
25	25	0.0028	10	10	2.4

TABLE I: Rate constants obtained from experimental data for *E-coli* [41, 42].

tRNA. The simplified cycle of the model ribosome has been shown in fig.5.

The typical values of the rate constants have been extracted from empirical data for the bacteria *E-coli* [41, 42]. Moreover, since there is no significant difference in the structures of the two elongation factors and since their binding mechanisms are also similar [5], we assume that the rate constants  $\omega_{h1}$  and  $\omega_{h2}$  are equal. The values of the rate constants used in our calculations are listed in table I.

By extending the TASEP, Lakatos et al.[43] developed a model where each particle is allowed to hop with one of the two different hopping probabilities when the target site is empty. The hopping probability per time step is  $q_2$  if the site belongs to a specific pre-selected subset of periodically arranged sites, but at all other sites the hopping takes place with the probability  $q_2$ . In other words, Lakatos et al. considered a model with *spatial* periodicities in the hopping rates.

In principle, our model of ribosomes (with 5 “internal” states) of size  $\ell = 1$  on a mRNA of  $L$  codons can be mapped onto an equivalent model (let us refer to this new version of our model as  $5R$  model) consisting of

$5L$  sites on which point particles (without any "internal" states) hop with appropriate rate constants. At first sight, it may appear that the  $5R$  model is equivalent to the TASEP-like model of Lakatos et al.[43] with spatially periodic hopping rates. But, that is not true because of the unusual nature of the interactions between the hypothetical particles in  $5R$  model; these hypothetical particles experience exclusion if and only if it is located at the sites  $5n$ , where  $n$  is any non-zero integer, and not otherwise. Moreover, the interaction is long-ranged in the sense that a particle located at  $5n$  cannot hop forward if any of the next 5 sites (from  $5n + 1$  to  $5(n + 1)$ ) in front of it is occupied. Furthermore, only one of the five sites from  $5n + 1$  to  $5(n + 1)$  can be occupied at any given instant of time.

### C. Quantities of interest

Note that the *number density*  $\rho$  of the ribosomes is given by  $N/L$  where  $N$  is the total number of the extended particles and  $L$  is the length of the lattice. Obviously, the lattice is fully covered when  $N\ell = L$  and, therefore, the maximum possible number density of the extended particles is  $\rho_{max} = 1/\ell$ . One can also define [14] the coverage density  $\rho_{cov} = N\ell/L$ . From now onwards, the term density would imply number density, if not stated otherwise.

In the context of ribosomal traffic, the position, average speed and flux of ribosomes have interesting interpretations in terms of protein synthesis. The position of a ribosome on the mRNA also gives the length of the nascent polypeptide it has already synthesized. The average speed of a ribosome is also a measure of the average rate of polypeptide elongation. The flux of the ribosomes gives the total rate of polypeptide synthesis from the mRNA strand, i.e., the number of completely synthesized polypeptides per unit time.

The lifetime of a typical eukaryotic mRNA is of the order of hours whereas the time taken to synthesize an entire protein by translating the mRNA is of the order of a few minutes. Consequently, most often protein synthesis takes place under steady-state conditions. Therefore, although we shall formulate time-dependent equations for protein synthesis, we shall almost exclusively focus on the steady-state properties of these models in this paper.

### D. Methods of calculation

Most of our analytical calculations have been performed in the mean-field approximation. In order to test the accuracy of the approximate analytical results, we have also carried out computer simulations of our model. Since we found very little difference in the results for systems size  $L = 300$  and those for larger systems, all of our production runs were carried out using  $L = 300$ . We have used random sequential updating which corre-

sponds to the master equations formulated for the analytical description. In each run of the computer simulations the data for the first *five million* time steps were discarded to ensure that the system, indeed, reached steady state. The data were collected in the steady state over the next *five million* time steps. Thus, each simulation run extended over a total of ten million time steps. For example, the average steady-state flux was obtained by averaging over the last five million time steps.

## V. RESULTS IN THE SPECIAL CASE $\ell = 1$

Typically, a single ribosome itself covers about twelve codons (i.e.,  $\ell = 12$ ), and interacts with others by mutual exclusion. However, as a first step, we consider the special case  $\ell = 1$ , with periodic boundary conditions. This is *not* equivalent to TASEP because of the incorporation of the biochemical cycle in the dynamics of the model. We set up the Master equations for the process of translation in this special case  $\ell = 1$ , and then solve them in the mean field approximation. We compare our analytical results with the corresponding numerical results which we obtain by computer simulations.

### A. Master equations in the special case $\ell = 1$

Let  $P_\mu(i)$  be the probability of finding a ribosome at site  $i$ , in the chemical state  $\mu$ . Also,  $P(i) = \sum_{\mu=1}^5 P_\mu(i)$ , is the probability of finding a ribosome at site  $i$ , in any state. The master equations (under the assumptions discussed above, and under the mean field approximation) are thus:

$$\frac{\partial P_1(i)}{\partial t} = \omega_{h2}(1 - P(i))P_5(i-1) + \omega_p P_2(i) - \omega_a P_1(i) \quad (4)$$

$$\frac{\partial P_2(i)}{\partial t} = \omega_a P_1(i) - (\omega_p + \omega_{h1})P_2(i) \quad (5)$$

$$\frac{\partial P_3(i)}{\partial t} = \omega_{h1}P_2(i) - k_2 P_3(i) \quad (6)$$

$$\frac{\partial P_4(i)}{\partial t} = k_2 P_3(i) - \omega_g P_4(i) \quad (7)$$

$$\frac{\partial P_5(i)}{\partial t} = \omega_g P_4(i) - \omega_{h2}(1 - P(i+1))P_5(i) \quad (8)$$

Mean field approximation has been made in writing these equations; this approximation has been assuming that the probability of there being a ribosome at site  $i$  is not affected by the presence or absence of other ribosomes at other sites.

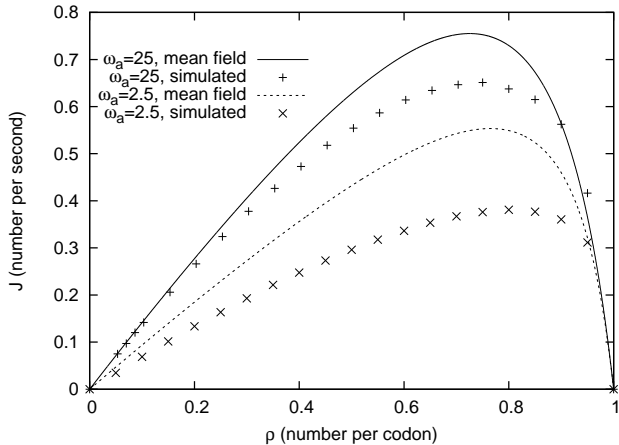


FIG. 6: Flux of ribosomes with  $\ell = 1$ , under periodic boundary conditions, plotted against density. The curves correspond to the analytical expressions obtained in the mean-field approximation whereas the discrete data points have been obtained by carrying out computer simulations. Values of all the parameters, except  $\omega_a$ , are same as those listed in table I.

### B. Steady state solution under periodic boundary condition for $\ell = 1$

In the steady state, all time derivatives vanish. Moreover, if periodic boundary conditions are imposed (i.e., the lattice effectively forms a ring) no site has any special status and the index  $i$  can be dropped. Solving the equations governing the process of protein elongation in the steady-state with periodic boundary conditions we get

$$P_5 = \frac{P}{1 + \Omega_{h2}(1 - P)} \quad (9)$$

where,

$$\Omega_{h2} = \omega_{h2}/k_{eff}. \quad (10)$$

with

$$\frac{1}{k_{eff}} = \frac{1}{\omega_g} + \frac{1}{k_2} + \frac{1}{\omega_{h1}} + \frac{1}{\omega_a} + \frac{\omega_p}{\omega_a \omega_{h1}} \quad (11)$$

Using the relation

$$J = \omega_{h2} P_5 (1 - P) \quad (12)$$

for the flux  $J$ , we get the steady-state flux

$$J = \frac{\omega_{h2} \rho (1 - \rho)}{1 + \Omega_{h2} (1 - \rho)} \quad (13)$$

where we have also used the fact that, in this case,  $P$  is identical to the global density  $\rho$  of the ribosomes in the system. Note that  $k_{eff}^{-1}$  is an effective time that incorporates the delays induced by the intermediate biochemical steps in between two successive hoppings of the

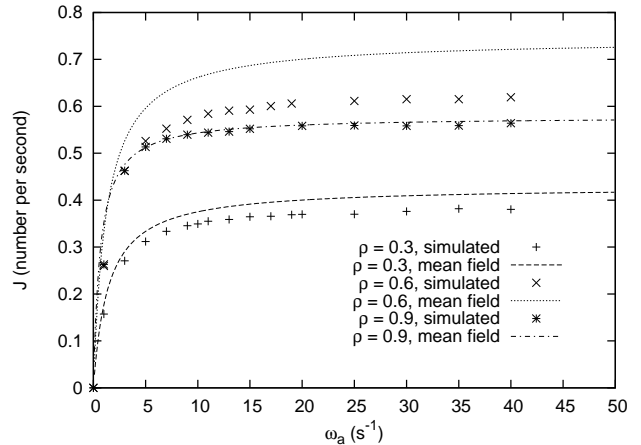


FIG. 7: Flux obtained from mean-field theory and computer simulations are plotted against  $\omega_a$  for three different densities of ribosomes in our model of protein synthesis. All other parameters are identical to those in fig.6.

ribosome from one codon to the next. In the special case  $k_{eff} \rightarrow \infty$ , where  $\omega_{h2} = q$  is non-zero and finite,  $\Omega_{h2} \rightarrow 0$ ; in that case  $P_5 \rightarrow P$  and  $J \rightarrow q\rho(1 - \rho)$  which is a well known result (2) for TASEP.

The mean-field estimate of the flux, which is given by the equation (13), has been plotted against  $\rho$  in figure 6 for various values of  $\omega_a$  along with the corresponding numerical data obtained from our computer simulations of the model. We find a fairly good agreement between the results of mean field approximation and computer simulations, especially in the low density region, and for large  $\omega_a$ . This is expected because when the density is low, the ribosomes are practically independent of each other. As the density increases, this is no longer the case, and the basic mean field estimate deviates more and more from the corresponding simulation data.

Both mean-field theory and computer simulations demonstrate that, for any given density  $\rho$ , higher  $\omega_a$  gives rise to larger  $J$ ; this is consistent with one's intuitive expectation because higher concentration of tRNA reduce the waiting time of the ribosome at a codon. Since none of the earlier theoretical models separately account for the two processes associated with the rate constants  $\omega_a$  and  $\omega_{h2}$ , this specific feature of protein synthesis could not be captured by those models. At small  $\omega_a$ , the availability of tRNA may, indeed, be the rate-limiting process during polypeptide elongation. But, if it increases to sufficiently large level, other processes may replace it as the rate-limiting step; this is evident from the saturation of the flux with increasing  $\omega_a$  shown in fig.7.

Note that the fundamental diagram shown in fig.6 is not symmetric about  $\rho = 1/2$  and the peak appears at a density larger than  $1/2$ . Moreover, the position of the peak shifts to higher densities with decreasing chemical rate constants. In the next subsection we compare our model with the Fukui-Ishibashi (FI) model [44] of ve-

hicular traffic to explain the physical origin of an this interesting generic feature of the fundamental diagrams in our model of ribosome traffic.

### C. Relation with models of vehicular traffic

The TASEP has been extended over the last fifteen years to develop many models to capture various aspects of vehicular traffic [7]. The Nagel-Schreckenberg (NS) model, which is essentially an extension of the TASEP, is the most widely used minimal model of vehicular traffic. It has been extended further to develop many other more realistic ‘‘particle-hopping’’ models which capture some phenomena that are not accounted for by the NS model. Fukui and Ishibashi [44] formulated a somewhat different minimal model which is less realistic than NS model for vehicular traffic.

Interestingly, the TASEP itself was developed originally [11] to model essential features of ribosome traffic. However, success of TASEP-like models of vehicular traffic and recent advances in molecular motors with the help of new powerful experimental techniques have led to a revival of the TASEP-like modelling strategy for traffic of wide varieties of molecular motors [8, 9]. These include, for example, traffic of cytoskeletal motors [45, 46, 47, 48, 49, 50, 51, 52] and that of motors that move on single-stranded DNA tracks [53, 54, 55], etc. Most of these focus on generic features rather than specific details of any particular motor.

#### 1. Comparison with the Fukui Ishibashi model

The FI model [44] is a ‘‘particle-hopping’’ model for vehicular traffic on single-lane highways. The update rules of the FI model are as follows:

If  $V_{max}$  or more sites in front of the  $i$ -th vehicle is empty at the time step  $t$ , then it has a probability  $1 - p$  to move forward by  $V_{max}$  sites and a probability  $p$  to move forward by  $V_{max} - 1$  sites in the time step  $t + 1$ . However, if only  $d$  sites ( $d < V_{max}$ ) in front of the  $i$ -th vehicle are empty at time  $t$  then it moves by  $d$  sites in the next time step. Note that, for general  $V_{max} > 1$ , in the FI model, (a) the increase of speed of the vehicles is not necessarily gradual and (b) the stochastic delay applies only to the vehicles that can move with the highest allowed velocity  $V_{max}$ . However, the FI model reduces to the NS model in the special case  $V_{max} = 1$  and the flux Vs density curve exhibits a maximum at the density  $\rho = 0.5$ . As  $V_{max}$  increases, the location of the maximum shifts to lower values of  $\rho$  as the vehicles feel stronger hindrance created by the leading vehicles. This trend of variation of the location of the maximum on the flux Vs density curve is also shared by the NS model for the same underlying mechanism.

Thus, the vehicles in the FI model are allowed to move by more than one site in each time step. The situation

in our model of ribosome traffic is just the opposite- the intermediate chemical states prevent the ribosome from moving even one site in one time step, because the ribosome may simply make a transition from one chemical state to another without moving from one codon to the next. In a sense, so far as the spatial movement of the ribosome is concerned, our model is like the FI model with fractional  $V_{max}$ , i.e.,  $V_{max} = \frac{1}{m}$ , where,  $m$  is the number of intermediate chemical states [82].

*In order to make a direct comparison of the two models, we consider the deterministic limit  $p = 0$  (i.e., hopping probability = 1) in the FI model and set the probabilities of all the transitions between various chemical states in our ribosome traffic model to unity. We now derive the fundamental relations for both these models (in the special cases mentioned) under mean-field approximations imposing periodic boundary conditions.*

Let  $P(i, t)$  be the probability of occupation of a the site  $i$ , at time  $t$ , by a vehicle. In the steady state, the probability that in a time step, a particle crosses site  $i$  is given by:

$$J = \sum_{a=0}^{n-1} P(i-a) \prod_{b=i-a+1}^{i+1} (1 - P(b)) \quad (14)$$

Moreover, owing to the periodic boundary condition, all sites are equivalent. Therefore,  $P(i) = \rho$ , independent of  $i$ , where  $\rho$  is the global density of the vehicles. The expression (14) for the flux can thus be summed to yield

$$J = (1 - \rho)[1 - (1 - \rho)^n] \quad (15)$$

The mean field flux for the ribosome model, in the special case where all the transitions probabilities have been set equal to unity, can simply be obtained from the general equations set up in section V. We quote the result for  $n = \frac{1}{m}$ , where  $m$  is the number of intermediates:

$$J = \frac{\rho(1 - \rho)}{1 + (m - 1)(1 - \rho)} \quad (16)$$

The mean field fundamental diagrams for FI model and those for our model of ribosome traffic have been plotted in figure 8. Increase of  $n$  in the FI model causes the density corresponding to the maximum flux to shift to lower values. Similarly, increase of  $m$  in the model of ribosome traffic causes this point to shift to higher values of density.

## VI. RESULTS IN THE GENERAL CASE WITH ARBITRARY $\ell$

Now we consider the general case of our model where the smaller subunit of each ribosomes has a length  $\ell > 1$ . *Position of such a ribosome will be referred to by the integer index of the lattice site covered by the leftmost site of*

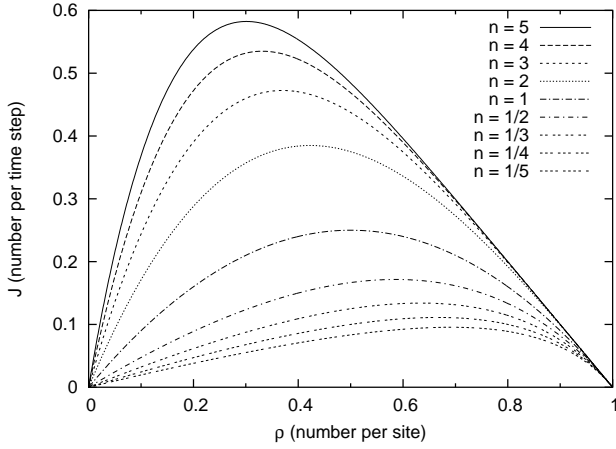


FIG. 8: Mean-field estimates of flux in the Fukui-Ishinashi model are plotted against the density of the vehicles for several different values of  $n$ . In the context of vehicular traffic only integer values of  $n$  are allowed; the fractional values of  $n$  are used only to establish the relation between the Fukui-Ishibashi model and our model of ribosome traffic.

*the smaller subunit.* Let  $P(\underline{i}|j)$  be the conditional probability that, given a ribosome at site  $i$ , there is another ribosome at site  $j$ . Then,  $Q(\underline{i}|j) = 1 - P(\underline{i}|j)$  is the conditional probability that, given a ribosome in site  $i$ , site  $j$  is empty. In the mean-field approximation, the Master equations for the probabilities  $P_\mu(i)$  are given by

$$\frac{\partial P_1(i)}{\partial t} = \omega_{h2}P_5(i-1)Q(\underline{i-1}|i-1+\ell) + \omega_p P_2(i) - \omega_a P_1(i) \quad (17)$$

$$\frac{\partial P_2(i)}{\partial t} = \omega_a P_1(i) - (\omega_p + \omega_{h1})P_2(i) \quad (18)$$

$$\frac{\partial P_3(i)}{\partial t} = \omega_{h1}P_2(i) - k_2 P_3(i) \quad (19)$$

$$\frac{\partial P_4(i)}{\partial t} = k_2 P_3(i) - \omega_g P_4(i) \quad (20)$$

$$\frac{\partial P_5(i)}{\partial t} = \omega_g P_4(i) - \omega_{h2}P_5(i)Q(\underline{i}|i+\ell) \quad (21)$$

Note that not all of the five equations (17)-(21) are independent of each other because of the condition

$$P(i) = \sum_{j=1}^5 P_j(i) = \frac{N}{L} = \rho \quad (22)$$

In our calculations below, we have used the equations (18)-(22) as the five independent equations.

### A. Steady state solution under periodic boundary condition for arbitrary $\ell$

If periodic boundary conditions are imposed, all the sites can be treated on equal footing in the steady state. Therefore, the corresponding flux of the ribosomes  $J$  can be obtained from

$$J = \omega_{h2}P_5Q(\underline{i}|i+\ell). \quad (23)$$

In order to proceed further, we need  $Q(\underline{i}|i+\ell)$ . Because of the translational invariance in the steady state, we have  $Q(\underline{i}|j) = Q(\underline{1}|j-i+1)$ . Therefore, we now calculate  $Q(\underline{1}|1+\ell)$ : given a ribosome at the site  $i=1$ , what is the probability that the site  $i=\ell+1$  is empty? Since it is given that the site  $i=1$  is occupied by a ribosome, the remaining  $N-1$  ribosomes must be distributed among the remaining  $L-\ell$  sites. Let us introduce the symbol  $Z(L, N, \ell)$  to denote the number of ways of arranging the  $N$  ribosomes and  $L-N\ell$  gaps. Obviously,

$$Z(L, N, \ell) = \frac{(N+L-N\ell)!}{N!(L-N\ell)!} \quad (24)$$

In case it is given that one ribosome occupies  $i=1$ , the total number of configurations would be  $Z(L-\ell, N-1, \ell)$ . Of these, we wish to find the number of those configurations where  $i=\ell$  also occupied; this is given by  $Z(L-2\ell, N-2, \ell)$ . Therefore, the probability that  $i=\ell$  is occupied, given that  $i=1$  is occupied, is given by

$$\begin{aligned} P(\underline{1}|\ell+1) &= \frac{Z(L-2\ell, N-2, \ell)}{Z(L-\ell, N-1, \ell)} \\ &= \frac{N-1}{L+N-N\ell-1} \end{aligned} \quad (25)$$

Hence,

$$Q(\underline{i}|i+\ell) = \frac{L-N\ell}{L+N-N\ell-1}. \quad (26)$$

In order to get the flux, we next calculate  $P_5$ . In the steady state, all time derivatives can be put to zero. Also, because of the periodic boundary conditions the index  $i$  can be dropped. Under these conditions, equations (18-22) can be solved to obtain:

$$P_5 = \frac{P}{1 + \frac{\Omega_{h2}(L-N\ell)}{L+N-N\ell-1}} \quad (27)$$

Using expressions (26) and (27) in (23) and the definition  $\rho = N/L$  for the number density, we get

$$J = \frac{\omega_{h2}\rho(1-\rho\ell)}{(1+\rho-\rho\ell) + \Omega_{h2}(1-\rho\ell)} \quad (28)$$

Note that  $J$  vanishes at  $\rho=0$  and for all  $\rho \geq \rho_{max} = 1/\ell$  because at the density  $\rho_{max}$  the entire mRNA is fully covered by ribosomes. In the special case  $\ell=1$ , the expression (28) reduces to the expression (13) for  $J$ .

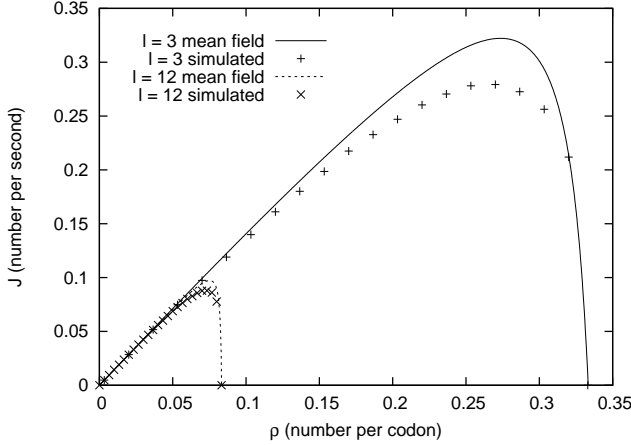


FIG. 9: Flux of ribosomes with  $\ell = 3, 12$ , under periodic boundary conditions, plotted against density. The curves correspond to the analytical expressions obtained in the mean-field approximation whereas the discrete data points have been obtained by carrying out computer simulations. Values of all the parameters, except  $\ell$ , are same as those in fig.6.

Moreover, in the special situation where  $k_{eff} \rightarrow \infty$ , but  $\omega_{h2} = q$  remains non-zero and finite,  $\Omega_{h2} \rightarrow 0$  and the expression (28) reduces to the well known expression (2) for flux in TASEP.

The flux obtained from (28) has been plotted in figure (9) for various values of  $\ell$ . This trend of variation with  $\ell$  was also observed in the pioneering work of MacDonald et al. [11] in their simpler model. By differentiating equation (28), we obtain that the density  $\rho^*$  corresponding to the maximum of the flux is the solution of the equation:

$$\rho^2 \ell (1 - \ell - \Omega_{h2} \ell) + 2\rho \ell (1 + \Omega_{h2}) - (1 + \Omega_{h2}) = 0 \quad (29)$$

and, hence,

$$\rho^* = \sqrt{\left(\frac{1 + \Omega_{h2}}{\ell}\right) \left[\frac{1}{\sqrt{\ell(1 + \Omega_{h2})} + 1}\right]} \quad (30)$$

We recover the equation (3) for  $\rho_m$  in the appropriate limit  $\Omega_{h2} \rightarrow 0$ . Our theoretical predictions in fig.9 are also in good agreement with the corresponding simulation data.

In order to see the effects of varying the rates of some of the biochemical transitions, we have plotted the fundamental diagram in fig.10 for two different situations, namely,  $\omega_{h1} = 10\omega_{h2}$  with  $\omega_{h2} = 10 \text{ s}^{-1}$  and  $\omega_{h2} = 10\omega_{h1}$  with  $\omega_{h1} = 10 \text{ s}^{-1}$ . The fundamental diagrams in these two situations turn out to be almost identical; this is a consequence of the fact that for the set of parameter ranges used in this figure, neither  $\omega_{h1}$  nor  $\omega_{h2}$  corresponds to the rate limiting process.

We have plotted the fundamental diagrams of the model in fig.11 for three different values of  $\omega_a$ , namely,  $\omega_a = 2.5 \text{ s}^{-1}$ ,  $\omega_a = 25 \text{ s}^{-1}$  and  $\omega_a = 250 \text{ s}^{-1}$

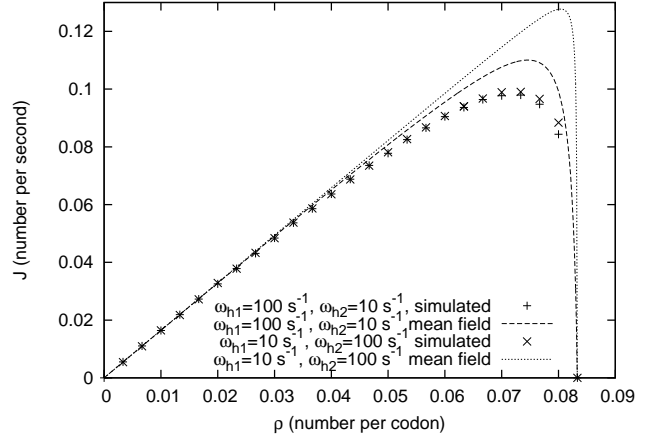


FIG. 10: Flux of ribosomes with  $\ell = 12$ , under periodic boundary conditions, plotted against density. The curves correspond to the analytical expressions obtained in the mean-field approximation whereas the discrete data points have been obtained by carrying out computer simulations. Values of all the parameters, except  $\omega_{h1}$  and  $\omega_{h2}$ , are identical to those in fig.6.

using both mean-field theory and computer simulations. The results show that at sufficiently small values of  $\omega_a$ , where the availability of the tRNA is the rate-limiting process, the flux increases rapidly with increasing  $\omega_a$ . However, the rate of this increase decreases with increasing  $\omega_a$  and, eventually flux essentially saturates when  $\omega_a$  is so large that the availability of tRNA is no longer the rate limiting process. Very similar trend of variation of flux with  $\omega_g$  is observed in fig.12 when  $\omega_g$  is varied over three orders of magnitude. In contrast, the flux has been observed to vary at significant rate even at the highest values of  $k_2$  when is varied over three orders of magnitude (see fig.13 indicating that saturation of flux with respect to  $k_2$  variation sets in at even higher values of  $k_2$ ).

## VII. RESULTS FOR OPEN BOUNDARY CONDITIONS

An open boundary condition is more realistic than periodic boundary conditions for describing ribosome traffic on mRNA. The new parameters which enter into the model are  $\alpha$  and  $\beta$  which we have already introduced in section IV. These are associated with initiation and termination of translation.

### A. Mean field analysis of steady state under open boundary conditions

In this subsection we calculate the flux of ribosomes (and, hence, the rate of protein synthesis) using a mean field theoretical approach similar to that developed by

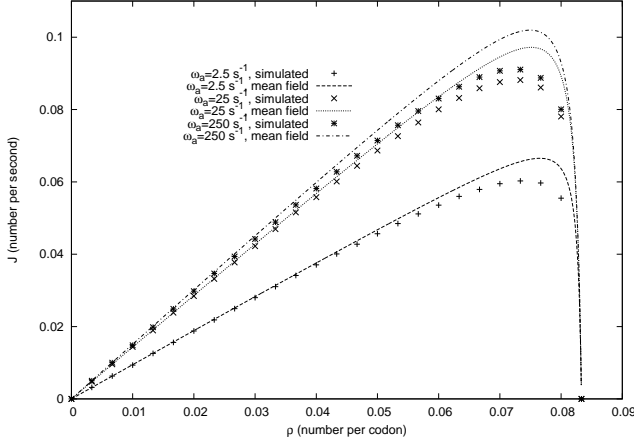


FIG. 11: Flux of ribosomes with  $\ell = 12$ , under periodic boundary conditions, plotted against density. The curves correspond to the analytical expressions obtained in the mean-field approximation whereas the discrete data points have been obtained by carrying out computer simulations. Values of all the parameters, except  $\omega_\alpha$  are identical to those in fig.6.

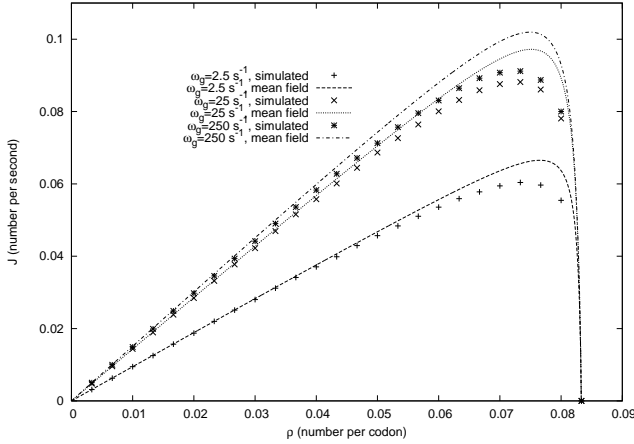


FIG. 12: Flux of ribosomes with  $\ell = 12$ , under periodic boundary conditions, plotted against density. The curves correspond to the analytical expressions obtained in the mean-field approximation whereas the discrete data points have been obtained by carrying out computer simulations. Values of all the parameters, except  $\omega_g$  are identical to those in fig.6.

Shaw et al. [15]. The approximation involved is that the conditional probability of site  $i + \ell$  being empty, given that site  $i$  has a ribosome in it, is replaced simply by the probability of site  $i$  being empty, given no other condition.

If  $P_i$  is the probability of there being a ribosome at site  $i$ , then the probability of there being a hole at site  $j$  is given by  $1 - \sum_{s=0}^{\ell-1} P_{j-s}$ . Also, since  $\alpha$  is the probability of attachment in time  $\Delta t$ , the probability of attachment

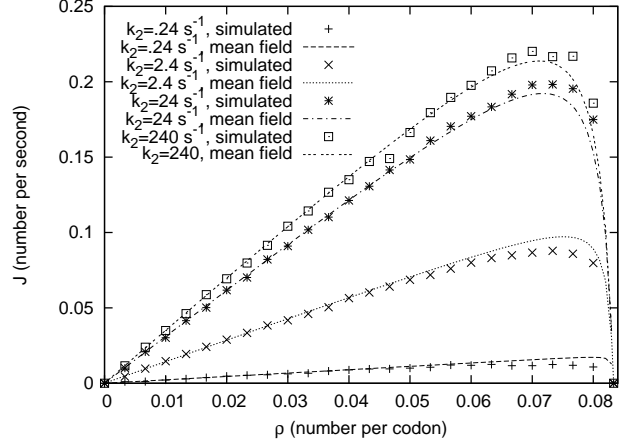


FIG. 13: Flux of ribosomes with  $\ell = 12$ , under periodic boundary conditions, plotted against density. The curves correspond to the analytical expressions obtained in the mean-field approximation whereas the discrete data points have been obtained by carrying out computer simulations. Values of all the parameters, except  $k_2$  are identical to those in fig.6.

per unit time (which we call  $\omega_\alpha$ ) is the solution to the equation  $\alpha = 1 - e^{-\omega_\alpha \times \Delta t}$ . It is now straightforward to set up the master equations for the probabilities  $P_\mu(i)$  in the mean-field approximation:

$$\frac{dP_1(1)}{dt} = \omega_\alpha(1 - \sum_{s=1}^{\ell} P(s)) + \omega_p P_2(1) - \omega_a P_1(1) \quad (31)$$

$$\frac{dP_1(i)}{dt} = \frac{\omega_{h2} P_5(i-1)(1 - \sum_{s=1}^{\ell} P(i-1+s))}{1 - \sum_{s=1}^{\ell} P(i-1+s) + P(i-1+\ell)} + \omega_p P_2(i) - \omega_a P_1(i) \quad (32)$$

$(i \neq 1)$

$$\frac{dP_2(i)}{dt} = \omega_a P_1(i) - (\omega_p + \omega_{h1}) P_2(i) \quad (33)$$

$$\frac{dP_3(i)}{dt} = \omega_{h1} P_2(i) - k_2 P_3(i) \quad (34)$$

$$\frac{dP_4(i)}{dt} = k_2 P_3(i) - \omega_g P_4(i) \quad (35)$$

$$\frac{dP_5(i)}{dt} = \omega_g P_4(i) - \frac{\omega_{h2} P_5(i)(1 - \sum_{s=1}^{\ell} P(i+s))}{1 - \sum_{s=1}^{\ell} P(i+s) + P(i+\ell)} \quad (36)$$

$(i \neq 5)$

$$\frac{dP_5(N)}{dt} = \omega_g P_4(N) - \beta P_5(N) \quad (37)$$

The flux is given by  $J = \omega_\alpha(1 - \sum_{s=0}^{\ell} P_s)$ . This flux has been computed numerically by solving equations (31-37); the results are shown by the continuous curves in figures 14(a) and 14(b). These mean-field estimates are in excellent agreement with the corresponding numerical data obtained from computer simulations of the model. Moreover, the rates of protein synthesis corresponding to the typical rate constants given in table I are in the same order of magnitude as those observed experimentally [1]. The average density profiles observed at several values of  $\omega_h$  and  $\alpha$  are also shown in the insets of figs.14(a) and (b), respectively.

Figures 14(a) and (b) show how the current gradually increases and, finally, saturates as  $\omega_h$  (in (a)) and  $\alpha$  (in (b)) increase; the saturation value of the current is numerically equal to the maximum current obtained in the corresponding closed system with periodic boundary conditions. The average density profiles in the insets of the figures 14(a) and (b) establish that the average density of the ribosomes *decreases* with increasing  $\omega_h$ , but *increases* with increasing  $\alpha$ , gradually saturating in both the cases. These observations are consistent with the scenario of phase transition from one dynamical phase to another, as predicted by the extremal current hypothesis which will be considered later in this section.

### B. Effects of inhomogeneity of the mRNA track of real gene sequences

So far we have been assuming perfect homogeneity of the mRNA track, in the sense that the transition rates are independent of the position of the ribosome along the strand. However, in real gene sequences, this assumption is not very realistic. First of all, different codons appear on a mRNA with different frequencies. Moreover, in a given cell, not all the tRNA species, which correspond to different codon species, are equally abundant. There are some codons which appear on mRNAs less frequently than other more common codons. Interestingly, because of evolutionary adaptations, the concentrations of tRNA species which correspond to rare codons are also proportionately low [56].

The effect of rare codons and the relative scarcity of corresponding tRNA on the rate of protein synthesis has been investigated both experimentally as well as theoretically [37, 38]. Rare codons become more effective in blocking ribosomes if these codons are arranged in a compact cluster rather than being dispersed uniformly all along the mRNA strand [18, 57]. Besides, amino acid starvation of a ‘‘hungry’’ ribosome can lead to a substitution of the required scarce amino acid species by a more readily available species thereby causing a translation error [38].

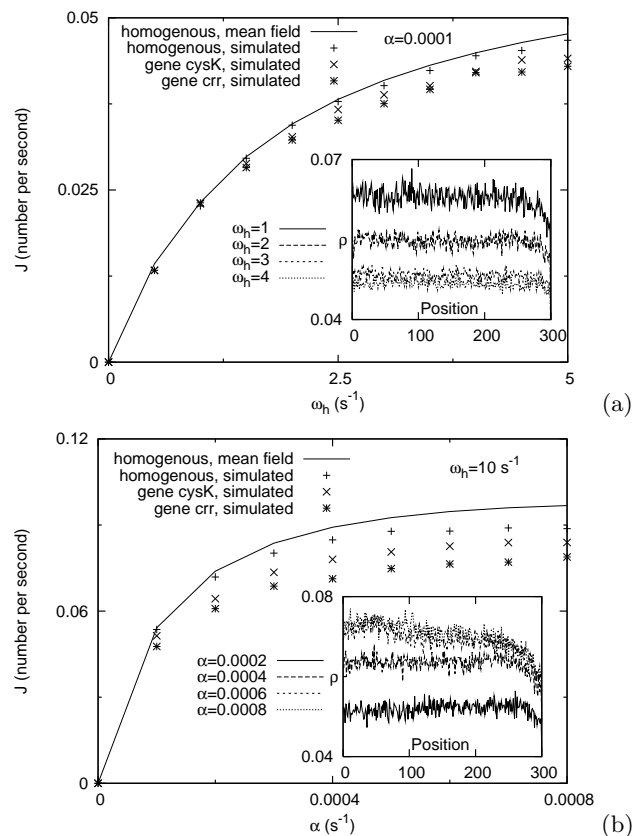


FIG. 14: Flux of ribosomes plotted against (a)  $\omega_h$  and (b)  $\alpha$  for the genes *crr* (170 codons) and *cysK* (324 codons) of *Escherichia coli* K-12 strain MG1655, as well as the corresponding curve for a homogenous mRNA strand of 300 codons. The insets show the average density profiles on a hypothetical *homogeneous* mRNA track for four different values of (a)  $\omega_h$  and (b)  $\alpha$ , for fixed  $\omega_\alpha = 25$  s<sup>-1</sup>.

Lot of work on TASEP with quenched random space-dependent hopping rates [60, 61, 62, 63, 64, 65, 66, 67, 68] and Brownian motors with quenched disorder [69, 70, 71, 72] have been reported. Similarly, effects of randomness on some stochastic chemical kinetic models of molecular motors have also been investigated [24, 25]. However, the nucleotide sequence on any real DNA or mRNA is not random. But, to our knowledge, for the inhomogeneous, but correlated, gene sequences no analytical technique is available at present for the calculation of the speed of the associated molecular motors. For example, all the theoretical schemes developed so far for RNA polymerase motors [73, 74] by taking into account the actual sequence of the specific DNA track, have to be implemented numerically. Even in the context of earlier TASEP-like models of protein synthesis, almost all the theoretical results on the effects of sequence inhomogeneities have been obtained by computer simulations [19]. Therefore, we have been able to study the effects of sequence inhomogeneities of real codon sequences on the rate of protein synthesis in our model only numerically by carrying out computer

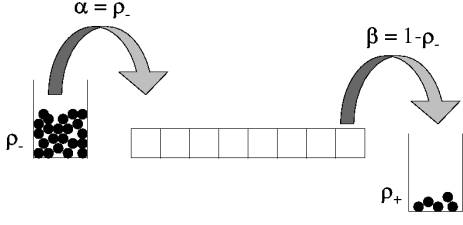


FIG. 15: Incorporating  $\alpha$  and  $\beta$  through two reservoirs with appropriate densities.

simulations.

We now extend our homogeneous model *assuming* that the rate constant  $\omega_a$  of the attachment of the tRNA to the site  $A$  of the ribosome is site-dependent (i.e., dependent on the codon species). More precisely, for a ribosome located at the  $i$ -th site, we multiply the numerical value of  $\omega_a$ , which we used earlier for the hypothetical homogeneous mRNA, by a multiplicative factor that is proportional to the relative concentration of the tRNA associated with the  $i$ -th codon [56, 58].

In our numerical studies, we focus on genes of *Escherichia coli* K-12 strain MG1655 [59]. We use the hypothesis mentioned above for the choice of the numerical values for the different species of codons. The results of our computer simulations are plotted with discrete points in fig.14. The lower flux observed for real genes, as compared to that for homogeneous mRNA, is caused by the codon specificity of the available tRNA molecules.

### C. Phase diagrams from extremal current hypothesis

We shall treat  $\alpha$ ,  $\omega_a$ ,  $\omega_{h1}$  and  $\omega_{h2}$  as the experimentally controllable parameters. We shall plot the phase diagrams of the model in planes spanned by pairs of these parameters. We shall plot these phase diagrams using equation (28), and an extremum principle which was originally introduced by Krug [75], stated in its general form by Popkov and Schütz [76] and effectively utilized in several later works [77, 78] in the context of driven diffusive lattice gas models.

In this approach, one imagines that the left and right ends of the system are connected to two reservoirs with the appropriate number densities  $\rho_-$  and  $\rho_+$  of particles (ribosomes) so that, assuming the same jumping rates as

in the bulk, the rates  $\alpha$  and  $\beta$  are incorporated into the model (see fig.15).

The extrema principle then relates the flux  $\mathcal{J}$  in the open system to the flux  $J(\rho)$  for the corresponding closed system (i.e., the system with periodic boundary conditions) with the same dynamics. In the limit  $L \rightarrow \infty$  [76], the extrema principle states that

$$\mathcal{J} = \begin{cases} \max J(\rho) & \text{if } \rho_- > \rho > \rho_+ \\ \min J(\rho) & \text{if } \rho_- < \rho < \rho_+ \end{cases} \quad (38)$$

In the present context of our model the expression (28) for  $J(\rho)$  exhibits a single maximum at  $\rho = \rho^*$  where  $\rho^*$  is given by the equation (30). Moreover, we take  $\rho_+ = 0$ , i.e.,  $\beta = 1$ , because we assume that the ribosome is released from the mRNA as soon as it reaches the stop codon; this is justified by the fact that, normally, termination is not the rate limiting step in the process of protein synthesis. Therefore, the extremal current hypothesis implies that in our model

$$\mathcal{J} = \max J(\rho) \text{ if } \rho_- > \rho^* \quad (39)$$

All the results derived in this section exploiting this extremum principle are approximate because the expression (28), which we use for the expression of  $J(\rho)$ , has been derived in the mean-field approximation. Next, following arguments similar those followed in all earlier applications of this extremum principle, we now derive the appropriate expressions for  $\rho_-$ .

Consider a closed system with  $L$  sites. Given that a sequence of  $\ell$  successive sites are empty, the total number of ways in which  $N$  ribosomes can be distributed over the remaining  $L - \ell$  sites is simply  $Z(L - \ell, N, \ell)$ . Of these,  $Z(L - 2\ell, N - 1, \ell)$  configurations have a ribosome in the adjacent  $\ell$  sites to the *left* of these empty  $\ell$  sites. Let us use the symbol  $\mathcal{P}(\underbrace{11\dots 1}_\ell | \underbrace{00\dots 0}_\ell)$  for the conditional

probability that, given a sequence of  $\ell$  successive empty sites, there will be a ribosome in the adjacent  $\ell$  sites to its *left*. Then, for the above considerations,

$$\mathcal{P}(\underbrace{11\dots 1}_\ell | \underbrace{00\dots 0}_\ell) = \frac{Z(L - 2\ell, N - 1, \ell)}{Z(L - \ell, N, \ell)} = \frac{N}{L - \ell + N - N\ell}. \quad (40)$$

In terms of the number density  $\rho$ , this probability can be expressed as

$$\mathcal{P}(\underbrace{11\dots 1}_\ell | \underbrace{00\dots 0}_\ell) = \frac{\rho}{\rho + 1 - \frac{\ell}{L} - \rho\ell}. \quad (41)$$

Moreover, solving the equations (31-37) we find

$$P_5 = \frac{1}{1 + \Omega_{h2}} \quad (42)$$

Therefore, if  $P^{jump}$  is the probability that, given a sequence of  $\ell$  successive empty sites, a ribosome will hop

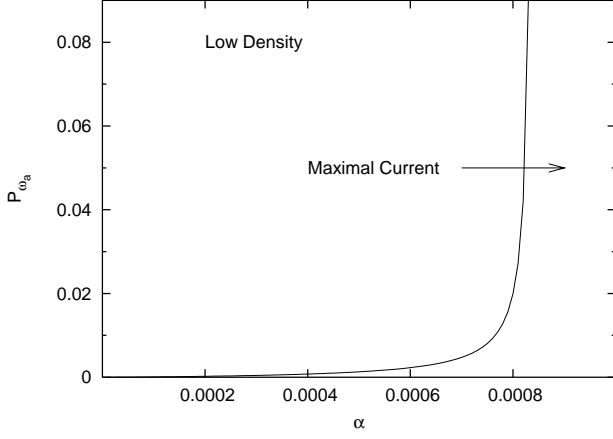


FIG. 16: Phase diagram in  $\alpha - P_{\omega_a}$  plane.  $P_{\omega_a}$  is the probability of attachment of a tRNA in the time  $\Delta t = 0.001$  s, and is related to  $\omega_a$  by equation (47). For this,  $\omega_{h1} = \omega_{h2} = 10 \text{ sec}^{-1}$ . To the left is the low density region, and to the right is the maximal current region

onto it in the next time step, we have

$$P^{jump} = \mathcal{P}(\underbrace{11\dots 1}_{\ell} | \underbrace{00\dots 0}_{\ell}) \times P_5 \times \omega_{h2}(\Delta t) \quad (43)$$

where  $\mathcal{P}(\underbrace{11\dots 1}_{\ell} | \underbrace{00\dots 0}_{\ell})$  and  $P_5$  are given by (41) and (42), respectively.

Now, going back to the open system,  $\rho_-$  is the solution of the equation  $\alpha = P^{jump}$  and, hence, we get

$$\rho_- = \frac{\alpha(1 - \frac{\ell}{L})(1 + \Omega_{h2})}{P_{\omega_h} - \alpha(1 + \Omega_{h2})(1 - \ell)} \quad (44)$$

where  $P_{\omega_h}$  is the probability of hydrolysis in the time  $\Delta t$ . In the special case  $k_{eff} \rightarrow \infty$  while  $\omega_{h2} = q$  remains finite and non-zero, i.e.,  $\Omega_{h2} \rightarrow 0$ ,  $\rho_- \rightarrow \frac{\alpha}{1 + (\ell - 1)\alpha}$ , which is identical to the expression derived earlier by Lakatos and Chou [13] for this special case.

Thus, the equation of the phase boundaries between the various phases have been obtained by solving the equation

$$\rho_-(\alpha, \omega_a, \omega_{h1}, \omega_{h2}) = \rho_*(\alpha, \omega_a, \omega_{h1}, \omega_{h2}) \quad (45)$$

numerically using  $\rho^*$  and  $\rho_-$  obtained, respectively, from equations (30) and (44); two typical phase diagrams have been plotted in figures 16 and 17 assuming [5, 41, 42]  $\omega_{h1} = \omega_{h2} = \omega_h$ . Each of these phase diagrams show two phases namely, a maximal current phase and another phase. In order to find out whether the latter is the low-density phase or the high-density phase, we studied the trend of variation of the density profile across the phase boundary (see fig.14). If the average density *decreases* and, finally, saturates in the maximal current

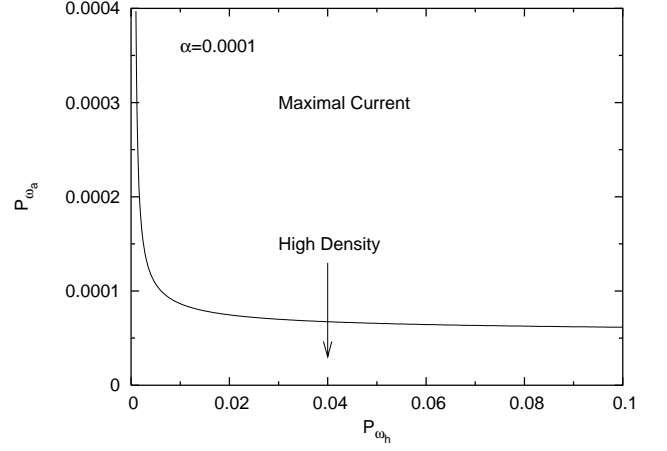


FIG. 17: Phase diagram in  $P_{\omega_h} - P_{\omega_a}$  plane.  $P_{\omega_h}$  is the probability of hydrolysis in the time  $\Delta t = 0.001$  s, and is related to  $\omega_h$  by equation (47). For this,  $\alpha = 0.0001$ . To the left is the low density region, and to the right is the maximal current region

phase (as observed in the inset of fig.14(a)) while the current reaches its maximum value, we identify it with the transition from the high-density phase to the maximal current phase (as in fig.16). On the other hand, gradual *increase* of the average density and its eventual saturation (as observed in the inset of fig.14(b)), while the current approaches its maximum value, indicates a transition from the low-density phase to the maximal current phase (as in fig.17).

Although the extremum current hypothesis [76] is believed to be exact, at least in the limit  $L \rightarrow \infty$ , our results on the phase boundaries are approximate because we have used the mean-field estimates (30) and (44) for  $\rho^*$  and  $\rho_-$ , respectively, in equation (45).

## VIII. SUMMARY AND CONCLUSION

The collective movement of ribosomes on a mRNA strand has been viewed for a long time as traffic flow of molecular motors [11, 12, 13, 14, 15, 16, 17, 18]. The physical properties of the non-equilibrium steady states of such systems of interacting “self-propelled” objects have been investigated in recent years using the techniques of non-equilibrium statistical mechanics [7, 8, 9, 10]. However, all the earlier TASEP-like models of ribosome traffic treat each ribosome as an “extended particle” (a hard rod) and capture the effects of the entire chemo-mechanical cycle that drives the translocation of the ribosome from one codon to the next by a single parameter, namely, hopping probability  $q$ .

In reality, a ribosome is not just a particle but one of the most complex natural nanomachines [3]. Thus, the underlying implicit assumption of TASEP type models of ribosome traffic is that the numerical value of  $q$

is determined by the rate-limiting step in the mechano-chemical cycle of a ribosome. Therefore, TASEP type models can successfully explain those collective properties of ribosome traffic which do not depend on the detailed mechano-chemical cycle of individual ribosomes. On the other hand, fundamental understanding of the interplay of the different steps of this cycle will not only provide deep insight into the mechanisms of regulation of gene expression, but may also find biomedical applications as ribosome is the target of many antibiotics [79].

In this paper we have developed a model of ribosome traffic during protein synthesis by explicitly incorporating all the major steps in the mechano-chemical cycle of each ribosome, in addition to the mutual exclusion of the ribosomes arising from their steric interactions. Thus, our work can also be viewed as an interesting biologically motivated extension of TASEP to an exclusion process for extended particles with “internal states”. Exclusion processes with “internal states” have begun receiving attention in very recent literature [80, 81].

We have calculated the flux of the ribosomes, which is directly related to the rate of protein synthesis, both analytically and numerically. Our approximate analytical results have been derived in the mean-field approximation and compared with the corresponding numerical data obtained by carrying out computer simulations. We have studied the model under both periodic and open boundary conditions. Moreover, in the latter case we have also calculated the average density profiles of the ribosomes on the mRNA track in all the dynamical phases of the system. Furthermore, we have determined the phase boundaries on the phase diagrams by using the extremum current hypothesis [76].

In contrast to all the earlier models of ribosome traffic, we have investigated the effects of varying the rate constants for the various steps of the mechano-chemical cycle of single ribosomes on the flux as well as on the density profiles. For each of the rate constants, we have shown that the current eventually saturates and the corresponding step of the mechano-chemical cycle is no longer rate limiting. Moreover, we have demonstrated that the sequence inhomogeneity of mRNA templates transcribed from real gene sequences slows down protein synthesis. We have illustrated this slowing down by showing the reduction in the flux in the case of a few real mRNA sequences for *E-coli* as compared to the flux of ribosomes on the corresponding hypothetical homogeneous track. Besides, we have calculated the flux in real time (unlike arbitrary units used in most of the earlier works). Our results for the rates of protein synthesis are in good agreement with the corresponding experimental data.

Following the traditional approach to phase diagrams of TASEP under open boundary conditions, all the earlier works on TASEP like models of ribosome traffic reported phase diagrams in the  $\alpha - \beta$  plane. But, we have plotted the phase diagrams in planes spanned by experimentally accessible parameters that include the concentrations of aa-tRNA and GTP-bound elongation factors. We hope the predictions of our theoretical model will stimulate further experimental studies for more accurate quantitative data.

**Acknowledgements:** One of the authors (DC) thanks Anatoly Kolomeisky, Alex Mogilner, Katsuhiko Nishinari and Gunter Schütz for comments and suggestions on an earlier version of the manuscript. DC also thanks Frank Jülicher and Stephan Grill for drawing his attention to the references [73, 74]. This work has been supported (through DC) by Council of Scientific and Industrial Research (CSIR), government of India.

### Appendix A: Rate constant versus probability

Consider a chemical reaction:  $A \rightarrow B$ , with a rate constant  $k$ . Thus,

$$\frac{d[B]}{dt} = k[A] = -\frac{d[A]}{dt} \quad (46)$$

Solving (46) gives

$$\frac{[A]_o - [A]}{[A]_o} = 1 - e^{-k\Delta t} \quad (47)$$

where  $[A]_o$  is the concentration of A at  $t = 0$ . The left hand side of (47) gives the fraction of A molecules reacted in time  $\Delta t$ , and is thus the probability that a *single* molecule of A will be transformed into B, in time  $\Delta t$ . If this time interval  $\Delta t$  is very small, we can expand the right hand side of equation (47). Differentiation this with respect to time gives the probability of transition per unit time:

$$\omega_{A \rightarrow B} = \frac{\partial}{\partial t} \lim_{t \rightarrow 0} (1 - e^{-kt}) = k \quad (48)$$

If  $P_A$  is the probability of finding the molecule in state A, then the final master equation, according to (48) is

$$\frac{\partial P_A}{\partial t} = -\omega_{A \rightarrow B} P_A \quad (49)$$

[1] B. Alberts, A. Johnson, J. Lewis, M. Raff, K. Roberts and P. Walter, *Molecular Biology of the Cell*, (4th edition) (Garland Publishing, 2002).

[2] See R. Phillips and S.R. Quake, Phys. Today, May issue,

p.38 (2006) for an elementary discussion.

[3] A. S. Spirin, *Ribosomes*, (Springer, 2000).

[4] A.S. Spirin, FEBS Lett. **514**, 2 (2002).

[5] R. A. Cross, Nature **385**, 18 (1997).

- [6] T.L. Hill. Proc. Natl. Acad. Sci. **64**, 267 (1969).
- [7] D. Chowdhury, L. Santen and A. Schadschneider, Phys. Rep. **329**, 199 (2000).
- [8] D. Chowdhury, A. Schadschneider and K. Nishinari, Phys. of Life Rev. **2**, 318 (2005).
- [9] A. Schadschneider, T. Pöschel, R. Kühne, M. Schreckenberg and D.E. Wolf, (eds.) Proc. of the international conference *Traffic and Granular Flow '05*, (Springer, 2006).
- [10] See the special issue of Physica A (guest eds. D. Chowdhury, A. Dutta and B.K. Chakrabarti) (2006) for the close similarities and crucial differences between biological traffic and vehicular traffic.
- [11] C. MacDonald, J. Gibbs and A. Pipkin, Biopolymers, **6**, 1 (1968).
- [12] C. MacDonald and J. Gibbs, Biopolymers, **7**, 707 (1969).
- [13] G. Lakatos and T. Chou, J. Phys. A **36**, 2027 (2003).
- [14] L.B. Shaw, R.K.P. Zia and K.H. Lee, Phys. Rev. E **68**, 021910 (2003).
- [15] L.B. Shaw, J.P. Sethna and K.H. Lee, Phys. Rev. E **70**, 021901 (2004).
- [16] L.B. Shaw, A.B. Kolomeisky and K.H. Lee, J. Phys. A **37**, 2105 (2004).
- [17] T. Chou, Biophys. J., **85**, 755 (2003).
- [18] T. Chou and G. Lakatos, Phys. Rev. Lett. **93**, 198101 (2004).
- [19] J.J. Dong, B. Schmittmann and R.K.P. Zia, arXiv: q-bio.QM/0606043 (2006).
- [20] G. M. Schütz, Phase Transitions and Critical Phenomena, vol. 19 (Acad. Press, 2001).
- [21] B. Schmittmann and R.K.P. Zia, in: *Phase Transition and Critical Phenomena*, Vol. 17, eds. C. Domb and J. L. Lebowitz (Academic Press, 1995).
- [22] J. Marro and R. Dickman, *Nonequilibrium Phase Transitions in Lattice models*, (Cambridge University Press, 1999).
- [23] K. Nishinari, Y. Okada, A. Schadschneider and D. Chowdhury, Phys. Rev. Lett. **95**, 118101 (2005).
- [24] Y. Kafri, D.K. Lubensky and D. R. Nelson, Biophys. J. **86**, 3373 (2004).
- [25] Y. Kafri and D.R. Nelson, J. Phys. Cond. Matt. **17**, S3871 (2005).
- [26] F. Jülicher, A. Ajdari and J. Prost, Rev. Mod. Phys. **69**, 1269 (1997).
- [27] P. Reimann, Phys. Rep. **361**, 57 (2002).
- [28] J. Howard, Curr. Biol. (2006).
- [29] H. F. Lodish, Nature **251**, 385 (1974).
- [30] A. A. Ferreira and F. C. Alcaraz, Phys. Rev. **65**, 052102 (2002).
- [31] G. Schönherr and G. M. Schütz, J. Phys. A **37**, 8215 (2004).
- [32] G. iSchönherr, Phys. Rev. E **71**, 026122 (2005).
- [33] J. Hiernaux, Biophys. Chem. **2**, 70 (1974).
- [34] R. Gordon, J. Theor. Biol. **22**, 515 (1969).
- [35] G. Vassert, J.E. Dumont and F. R. L. Canbtraine, Biochim. Biophys. Acta, **247**, 471 (1971).
- [36] G. von Heijne, L. Nilsson and C. Blomberg, Eur. J. Biochem. **92**, 397 (1978).
- [37] J.E. Bergmann and H.F. Lodish, J. Biol. Chem. **254**, 11927 (1979).
- [38] C. B. Harley, J. W. Pollard, C. P. Stanners and S. Goldstein, J. Biol. Chem. **256**, 10786 (1981).
- [39] M.A. Gilchrist and A. Wagner, J. Theor. Biol. **239**, 417 (2006).
- [40] S. Takyar, R.P. Hickerson and H.F. Noller, Cell **120**, 49 (2005).
- [41] R.C. Thompson, D.B. Dix and J.F. Eccleston, J. Biol. Chem. **255**, 11088 (1980).
- [42] K.M. Harrington, I.A. nazarenko, D.B. Dix, R.C. Thompson and O.C. Uhlenbeck, Biochem. **32**, 7617 (1993).
- [43] G. Lakatos, T. Chou and A. Kolomeisky, Phys. Rev. E **71**, 011103 (2005).
- [44] M. Fukui, Y. Ishibashi, J. Phys. Soc. Jpn., **65**, 1868 (1996).
- [45] R. Lipowsky, S. Klumpp and T.M. Nieuwenhuizen, Phys. Rev. Lett. **87**, 108101 (2001).
- [46] R. Lipowsky and S. Klumpp, Physica A **352** 53 (2005) and references therein.
- [47] R. Lipowsky, Y. Chai, S. Klumpp, S. Liepelt and M. J.I. Mller, Physica A (2006) in press and references therein.
- [48] A. Parmeggiani, T. Franosch and E. Frey, Phys. Rev. Lett. **90**, 086601 (2003).
- [49] A. Parmeggiani, T. Franosch and E. Frey, Phys. Rev. E **70**, 046101 (2004).
- [50] E. Frey, A. Parmeggiani and T. Franosch, Genome Inf. **15**, 46 (2004) and references therein.
- [51] M.R. Evans, R. Juhasz and L. Santen, Phys. Rev. E **68**, 026117 (2003).
- [52] V. Popkov, A. Rakos, R.D. Williams, A.B. Kolomeisky and G.M. Schütz, Phys. Rev. E **67**, 066117 (2003).
- [53] M.D. Betterton and F. Jülicher, Phys. Rev. Lett. **91**, 258103 (2003).
- [54] M.D. Betterton and F. Jülicher, Phys. Rev. E **71** 011904 (2005).
- [55] M. D. Betterton and F. Jülicher, J. Phys. Condens. Matter, **17**, S3851 (2005).
- [56] S.G.E. Andersson and C.G. Kurland, Microbiol. Rev. **54**, 198 (1990).
- [57] S. Zhang, E. Goldman and G. Zubay, J. Theor. Biol. **170**, 339 (1994).
- [58] J. Solomovici, T. Lesnik and C. Reiss, J. Theor. Biol. **185**, 511 (1997).
- [59] see <http://www.genome.wisc.edu/sequencing/k12.htm>
- [60] S.A. Janowsky and J.L. lebowitz, Phys. Rev. A **45**, 618 (1992).
- [61] G. Schütz, J. Stat. Phys. **71**, 471 (1993).
- [62] G. Tripathi and M. Barma, Phys. Rev. Lett. **78**, 3039 (1997); Phys. Rev. E **58**, 1911 (1998).
- [63] S. Goldstein and E.R. Speer, Phys. Rev. E **58**, 4226 (1998).
- [64] K. M. Kolwankar and A. Punnoose, Phys. Rev. E **61**, 2453 (2000).
- [65] R. J. Harris and R.B. Stinchcombe, Phys. Rev. E **70**, 016108 (2004).
- [66] C. Enaud and B. Derrida, Europhys. Lett. **66**, 83 (2004).
- [67] R. Juhasz, L. Santen and F. Igloi, Phys. Rev. Lett. **94**, 010601 (2005).
- [68] M. Barma, in ref.[10].
- [69] T. Harms and R. Lipowsky, Phys. Rev. Lett. **79**, 2895 (1997).
- [70] F. Marchesoni, Phys. Rev. E **56**, 2492 (1997).
- [71] M.N. Popescu, C.M. Arizmendi, A.L. Salas-Brito and F. Family, Phys. Rev. Lett. **85**, 3321 (2000).
- [72] Y. Jia, S.N. Yu and J.R. Li, Phys. Rev. E **63**, 052101 (2001).
- [73] L. Bai, A. Shundrovsky and M.D. Wang, J. Mol. Biol. **344**, 335 (2004).
- [74] V.R. Tadigotla, D.O. Maoileidigh, A.M. Sengupta, V.

- Epshtein, R.H. Ebright, E. Nudler and A.E. Ruckenstein, Proc. Nat. Acad. Sci. USA, **103**, 4439 (2006).
- [75] J. Krug, Phys. Rev. Lett. **67**, 1882 (1991).
- [76] V. Popkov and G. Schütz, Europhys. Lett. **48**, 257 (1999).
- [77] J. Hager, J. Krug, V. Popkov and G. Schütz, Phys. Rev. E **63**, 056110 (2001).
- [78] J. Hager, Phys. Rev. E **63**, 067103 (2001).
- [79] T. Hermann, Curr. Op. in str. biol. **15**, 355 (2005).
- [80] T. Reichenbach, T. Franosch and E. Frey, Phys. Rev. Lett. **97**, 050603 (2006).
- [81] F. Tabatabaei and G. M. Schütz, cond-mat/0608147 (2006).
- [82] In traffic theory  $V_{max}$  is an integer; in order to avoid confusion, we shall use the symbol  $n$  in place of  $V_{max}$  in the remaining part of this subsection